Separation Science and Technology
Publication details, including instructions for authors and subscription information:
http://www.informaworld.com/smpp/title~content=t713708471

Profile of Chemical Potential in Pressure-Driven Membrane Processes Accompanied by Gel-Enhanced Concentration Polarization

Sergey P. Agashichev[a]
[a] Research Center, ADWEA, Abu Dhabi, United Arab Emirates

To cite this Article Agashichev, Sergey P.(2009) 'Profile of Chemical Potential in Pressure-Driven Membrane Processes Accompanied by Gel-Enhanced Concentration Polarization', Separation Science and Technology, 44: 5, 1144 — 1163
To link to this Article: DOI: 10.1080/01496390902729072
URL: http://dx.doi.org/10.1080/01496390902729072

Separation Science and Technology, 44: 1144–1163, 2009

ISSN: 0149-6395 print/1520-5754 online
DOI: 10.1080/01496390902729072

Taylor & Francis
Taylor & Francis Group

Profile of Chemical Potential in Pressure-Driven Membrane Processes Accompanied by Gel-Enhanced Concentration Polarization

Sergey P. Agashichev
Research Center, ADWEA, Abu Dhabi, United Arab Emirates

Abstract: A model for distribution of chemical potential and concentration polarization enhanced by gel accumulated on membrane surface has been proposed. It provides distribution of chemical potential and concentration in the liquid phase and within the gel layer. The model allows analyzing the influence of thickness of fouling gel layer on the CP degree, surface concentration and chemical potential.

The model is based on the following assumptions:

1. process is accompanied by accumulation of gel layer at membrane surface along with concentration polarization;
2. diffusion layer and deposited gel consist of different components and these layers are characterized by different values of diffusivity coefficients;
3. correlation for effective hindered back diffusion coefficient within deposited layer is adopted from [Boudreau, *Geochim. Cosmochim. Acta*, **60**, 1996];
4. transverse transport is based on the following mechanisms: convection due to pressure difference and back diffusion owing to concentration gradient.

The following conclusions have been drawn: (A) diffusion resistance within the gel layer is getting dominant and cannot be ignored; (B) In the presence of a gel layer the membrane surface concentration, C_{1M}, is enhanced due to hindered back diffusion of salt ions that in turn, results in growth of osmotic pressure and chemical potential at the membrane surface. It provides elevated salt concentration in permeate and decreases

Received 13 July 2008; accepted 13 November 2008.
Address correspondence to Sergey P. Agashichev, Research Center, ADWEA, PO Box 54111, Abu Dhabi, United Arab Emirates. Fax: 971(2)665.83.74. E-mail: spagashichev@adwea.ae

the net driving force; (C) Analysis of calculated data indicates high sensitivity of CP degree to coefficient of hindered back diffusion within gel layer.

Keywords: Enhanced concentration polarization, gel polarization, hindered diffusion, reverse osmosis

INTRODUCTION AND FORMULATION OF THE PROBLEM

Reverse osmosis and nano-filtration are accompanied by colloidal or biofouling along with concentration polarization (CP) due to salt ions. Even pretreated water contains dissolved natural organics, colloids, aggregated organics, and residual suspended matter that make unavoidable gel accumulation. These phenomena cause a decline of permeability and decrease of salt rejection. The RO process accompanied by organic, bio, or colloidal fouling is characterized by a higher degree of CP that can decrease the level of transmembrane flux drastically. According to data in (1,2) the growing colloid deposits may enhance or exacerbate concentration polarization that, in turn, causes for more flux decline than could be explained by the hydraulic resistance of the colloid deposit layer itself. Molecular diffusion is inhibited within the deposited gel or cake layer because of decreased diffusivity coefficient within this layer. According to (1,3), the permeate flux decline in RO and NF processes is not caused by hydraulic resistance of the colloidal cake layer itself, but rather due to cake-enhanced osmotic pressure. It was reported (3), that the decline in salt rejection when colloidal fouling occurs was much more substantial for NF than for the RO membranes. The impact of ionic strength on colloidal fouling and in turn on the permeate flux decline and salt rejection was underlined. Permeate flux decline was attributed to the so-called "cake-enhanced osmotic pressure." According to data (3), salt rejection of the NF membranes dropped sharply from 84% to 20% when the concentration factor exceeded 1.5. Combined influence of natural organic matter (NOM) and colloidal particles on nano-filtration membrane fouling was considered in (4) Further investigation of enhancement of CP and osmotic pressure caused by accumulation of gel, cake, or biofilm on the membrane surface was done in (5–8).

According to the study (5), a dramatic increase of CP and loss in driving force via the enhanced osmotic pressure rather than through an additional hydraulic resistance, impact if biofouling on deterioration of membrane performance was considered in (6). According to their study biofilm deteriorates membrane performance by increasing both the

trans-membrane osmotic pressure and the hydraulic resistance. Bacterial cells on the membrane hinder the back diffusion of salt, which results in elevated osmotic pressure on the membrane surface and therefore decrease in permeate flux and salt rejection. On the other hand, EPS contributes to the decline in membrane water flux by increasing hydraulic resistance to permeate flow. Impact of NOM fouling on flux decline in NF was considered in (7), where the effect of ionic strength on specific resistance of cake was analyzed. It was concluded that increased cake resistance is consistent with more compact, less porous cake. Influence of bio-fouling on boron removal by nanofiltration and reverse osmosis membranes was reported in (8). Biofilm- enhanced concentration polarization in NF is accompanied by decline of degree of boron rejection from 44 to 13% of its initial value depending upon initial concentration of boron. These effects of biofilm growth are attributed to both an increase of hydraulic resistance to permeate flow and enhanced concentration polarisation near the membrane surface

Gel or cake layer accumulated at the membrane surface has an impact on hydrodynamic and mass-transfer characteristics of the process. Diffusion layer and deposited gel consist of different components which are characterized by different values of diffusivity.

Relying upon published studies one can conclude that an impact of the fouling layer is strongly influenced by its nature and morphology, namely the layer built of biocells and suspended matters with high porosity represents diffusion resistance because of the enhancement of osmotic pressure within this layer, while the compact layer consisting of organic macromolecules that forms a dense cross-linked fouling represents hydraulic resistance to permeate as well.

Many existing methods of modeling ignore any deformation of concentration profile within gel layer. Accounting of concentration polarization within the gel layer is becoming essential for design and analysis of RO and NF processes if membrane fouling takes place. Conventional techniques of calculations take into consideration only the hydrodynamic characteristics namely permeability and hydraulic resistance of the layer itself, while the diffusion resistance (or the enhancement of osmotic pressure within the gel layer) remains outside the scope of the studies. However, it is the diffusion resistance within the gel layer that can be a factor that the process is influenced by. (This phenomenon is explained by the difference in diffusivity coefficients in liquid phase and within the layer). This simplification is embedded into many existing software that makes the CP degree and diffusion resistance within the gel layer to be underestimated and therefore gives inaccurate design value of the transmembrane flux.

Distribution of concentration and chemical potential within the diffusion and gel layer is a measure of transport resistance that makes

essential their estimation for analysis and design of the processes. The structure of cake and its specific resistance are influenced by ionic strength at the membrane surface. A mathematical solution proposed in the previous study (9) can be applied for analysis of gel-enhanced concentration polarization in thin channel RO elements. This paper represents an attempt at further development of the model of profile of concentration and chemical potential within diffusion and deposited gel layers. Modeling of these phenomena is essential in design of the process and analysis of experimental and pilot results.

THEORY

Premises and Assumptions of the Model

An elementary parallelepiped as a fragment of symmetric plate-and-frame configuration of the membrane system was selected as a control volume. Balance equations were written over the control volume. The fluid is assumed to be incompressible, continuous, and isothermal with a uniform density field under the steady-state (time independent) conditions. The membrane charge density is ignored.

The considered process is accompanied by accumulation of the gel or the cake layer at the membrane surface along with concentration polarization. Conceptual illustration of the gel or cake enhanced concentration polarization is shown in Fig. 1. For the mathematical analysis to be simplified, the channel was subdivided into three zones according to the behavior of the concentration profile: (A), (B), and (C) respectively. Zone (A) covers the core of the channel where the concentration remains constant; zone (B) covers the diffusion layer and zone (C) includes the gel layer. A simplified model including two zones was presented in (9).

Transverse transport is based on the following mechanisms: convection due to pressure difference and back diffusion owing to concentration gradient. These transport sub-constituents are shown in Fig. 1. Analysis of CP in two-dimensional flow is based on the following governing equation.

$$\frac{\partial(uc)}{\partial x} + \frac{\partial}{\partial z}\left[Vc - D\left(\frac{\partial c}{\partial z}\right)\right] = 0 \tag{1}$$

This equation assumes convection in the longitudinal direction and diffusion and convection in the transverse direction. Within the selected control area all the characteristics are assumed to be independent upon longitudinal coordinate. For laminar regime in thin channel RO element,

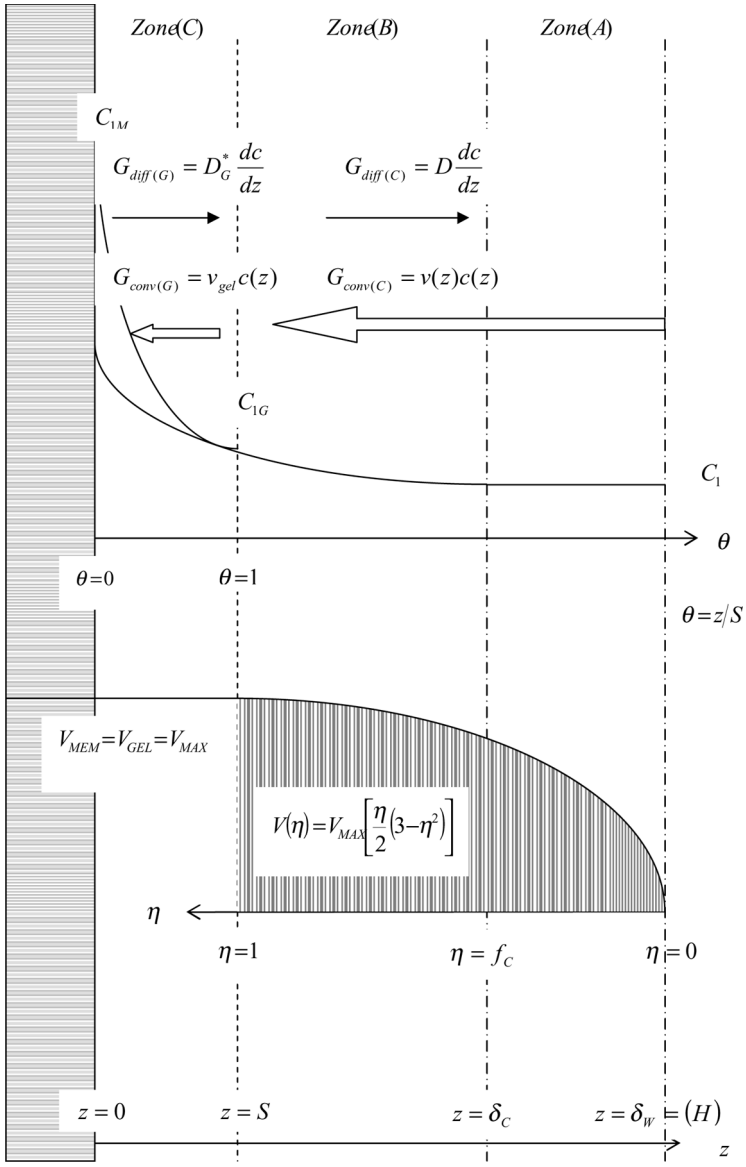

Figure 1. Conceptual illustration of the "gel enhanced" concentration profile (Concentration core, diffusion layer and gel).

the longitudinal convection can be ignored. Taking into consideration the orientation of axes shown in Fig. 1, the transport equation (1) can be written as follows.

$$Vc + D\frac{dc}{dz} = 0 \tag{2}$$

Where V- transverse flux; D- diffusivity; and C- local concentration (see Fig. 1). The first term on the left hand side represents convective flux towards membrane; the second one describes the back diffusion.

For the mathematical treatment to be simplified, the dimensionless variables η and θ were introduced.

The first dimensionless variable, η, ranges from $\eta = 0$ at the centerline to $\eta = 1$ at the gel (or cake) surface.

$$\eta = \frac{(H - z)}{(H - S)} \tag{3}$$

The η- variable is used for modeling characteristics in liquid phase, (see Fig. 1).

The second dimensionless variable, θ, ranges from $\theta = 0$ at the membrane surface to $\theta = 1$ at the upper surface of the gel (or cake) layer.

$$\theta = \frac{z}{S} \tag{4}$$

The θ- variable is used for modeling characteristics within the deposited gel layer, (see Fig. 1). Further analysis implies the following premises and simplifying assumptions.

Transverse velocity, $V(\eta)$, was approximated by parabolic function based on the function proposed by Berman, (10).

$$V(\eta) = V_{MAX}\left[\frac{\eta}{2}\left(3 - \eta^2\right)\right] \tag{5}$$

Transverse velocity varies from, $V_{(\eta=0)} = 0$, at the centerline to its maximum value $V_{(\eta=1)} = V_{MAX}$ at the gel surface. The transverse velocity is assumed to be constant through membrane and gel layer, (see Fig. 1).

$$V_{GEL} = V_{MEMBR} = V_{MAX} \tag{6}$$

Coefficient of Hindered Back Diffusion within Deposited Gel Layer

The considered process is accompanied by accumulation of gel or cake layer at the membrane surface. Hydraulic resistance of this layer is negligible within the range of porosity considered in this study. For the mathematical analysis to be simplified the deposited layer with

continuous structure is represented as equivalent layer formed by granulated particles characterized by definite value of apparent porosity-ε. (This granulated layer is assumed to be equivalent to real continuous layer and it has to be characterized by the same value of apparent diffusivity D^*. This layer represents an additional diffusion resistance). Different values of diffusivity in liquid phase and within the gel or cake layer are assumed in the model. This phenomenon is referred to as gel enhanced concentration polarization. Diffusivity within the layer is referred to as hindered back diffusion. For modeling to be simplified the gel layer was represented as a granulated layer characterized by equivalent diffusivity. The correlation for effective diffusion coefficient within the granulated cake layer proposed by Boudreau, (11) is used.

$$D^* = \frac{\varepsilon}{1 - \ln \varepsilon^2} D \tag{7}$$

Where: D^*-the effective diffusion coefficient in layer; D- the solute diffusivity in bulk; ε- porosity of deposited layer, (11).

Over the range of typical porosity the effective diffusion coefficient may be reduced to between 10 and 40% of the bulk diffusion coefficient that results in significantly enhanced salt concentration at the membrane surface, (1). Influence of sediment characteristics such as tortuosity and porosity on diffusive transport of ions and molecules is considered in (12).

Diffusion resistance to transport can be subdivided into two terms namely, resistance within the diffusion layer and resistance within the gel layer.

Concentration profile is shown in Fig. 1, where three zones (A), (B), and (C) characterized by different functional behavior of the profile are shown. The concentration remains constant equal C_1 within the core of the channel (zone A), that ranges from the centerline to the upper boundary of the diffusion layer, see Fig. 1. Within the diffusion layer (zone B) the concentration ranges from C_1 at its upper boundary to C_{1G} at the gel surface. An essential growth of concentration takes place within the gel layer (zone C) that is caused by hindered diffusion. The concentration ranges from C_{1G} at the gel surface to C_{1M} at the membrane. This model implies that the mathematical formulation of concentration profiles remains the same at any cross section along the channel assuming that the thickness of the viscous layer δ_W is assumed to be equal to half-height of the channel, H, see Fig. 1. According to (13), the ratio of diffusion to the viscous layer was assumed to be

$$\frac{\delta_C}{\delta_W} \approx Sc^{-1/3} \tag{8}$$

For considered case this ratio can be expressed in dimensionless form as follows

$$\frac{\delta_C}{\delta_W} \approx 1 - f_C \tag{9}$$

Chemical potential of solute μ_i related to activity a_i by

$$\mu_i = \mu_i^0 + RT \ln a_i \tag{10}$$

Where μ^0- potential at reference state,
Implying an ideal behavior of solution where $a_i = c_i$, Eq. (10) gives

$$\mu_i(z) = \mu_i^0 + RT \ln C_i(z) \tag{11}$$

Chemical potential within the concentration core is assumed to be position-independent and equal to the reference value at the centerline, $\mu_{\eta=0}$, or the reference state potential μ^0.

$$\mu_{\eta=0} = \mu_{\eta=f} = \mu^0 \tag{12}$$

Thermodynamic equilibrium at the gel surface is assumed to take place.

$$\mu_{\eta=1} = \mu_{\theta=1} \tag{13}$$

The first derivative of chemical potential, $-(d\mu/dz)_{P,\ T}$, represents an effective thermodynamic force, (14). For position-dependent concentration it can be expressed using Eq. (11)

$$\frac{d\mu_i}{dz} = RT \frac{d}{dz}[\ln C_i(z)] \tag{14}$$

Modeling

According to assumed transport mechanisms the cross area of the channel was subdivided into three zones, (A) and (B) and (C) covering the concentration core, the diffusion layer, and gel, respectively, (see Fig. 1). Zone (A) ranges from $z = \delta_C$ to $z = H$. There is no concentration gradient within the core. Concentration and chemical potential remains constant and equal to C_1 and μ_1, respectively, (see Assumptions). Transverse transport within zones (B) and (C) based on Eq. (2) is characterized by different values of diffusivities.

Profile of Concentration and Chemical Potential within Diffusion Layer (Zone B)

The diffusion layer (zone B) ranges from z = S to z = δ_C. Within this layer transverse velocity varies from $V = V_{(\eta=f)}$ to $V = V_{\max(\eta=1)}$ and approximated by parabolic function (see Eq 5).

For the diffusion layer where concentration and transverse velocity are characterized by functions $C(z)$ and $V(z)$, Eq. (2) can be expressed as follows:

$$V(z)C(z) + D\frac{dC}{dz} = 0 \tag{15}$$

Boundary conditions at the upper boundary of diffusion layer (see Fig. 1) are:

$$C_{(Z=\delta_C)} = C_1$$

And at the upper boundary of the deposited layer:

$$C_{(Z=S)} = C_{1G}$$

Rearrangement of Eq. (15) gives the following function for concentration profile within diffusion layer. (See Appendix A)

$$\frac{c(\eta)}{C_1} = \exp\left\{\frac{V_{MAX}(H-S)}{8D}[6(\eta^2 - f^2) - (\eta^4 - f^4)]\right\} \tag{16}$$

The profile based on Eq. (16) is shown in Fig. 2. At $\eta = 1$ we get the CP module at the boundary between the diffusion and gel layers

$$\left(\frac{C_{1G}}{C_1}\right)_{\eta=1} = \exp\left[\frac{5\ V_{MAX}(H-S)}{8D}(1-f^2)(5+f^2)\right] \tag{17}$$

For the case $Sc = 555$, it gives $f = 1 - Sc^{-1/3} = 0.878$, the CP module $(C_{1G}/C_1)_{\eta=1} = 1.3$.

The first derivative of chemical potential, $-(d\mu/dz)_{P,T}$, represents an effective thermodynamic driving force arising from a concentration gradient. Rearrangement and differentiation of Eq. (17) with respect to

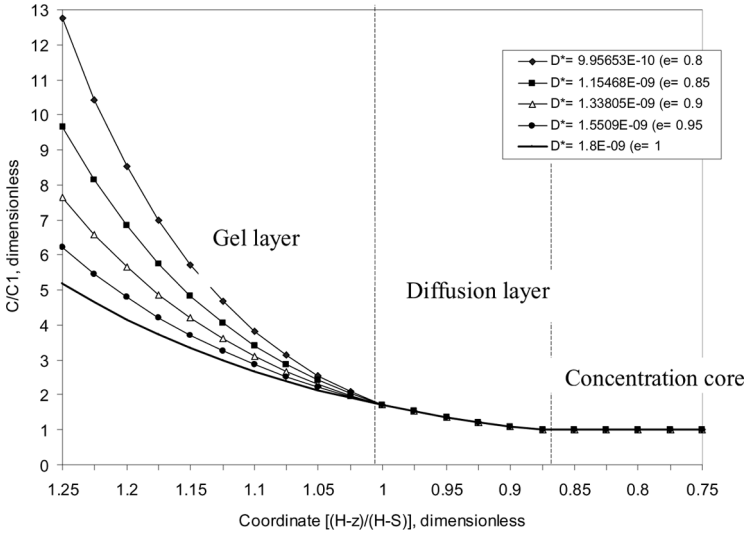

Figure 2. Calculated projections of concentration at different values of effective diffusivity within the gel layer (calculation for $D^*$is based on Eq. (7). Input data: $D = 1.8 \cdot 10^{-9}\,\mathrm{m^2/s}$; $V_{MEMBR} = 5 \cdot 10^{-6}\,\mathrm{m/s}$; $\mathrm{H} = 0.001\,\mathrm{m}$; $\mathrm{S} = 2 \cdot 10^{-4}\,\mathrm{m}$).

the η-variable gives the relation between concentration and the thermodynamic driving force.

$$\frac{d\mu_i}{d\eta} = RT\frac{d}{d\eta}[\ln\, c_i(\eta)] \tag{18}$$

Combining (18) with the first derivative of concentration profile, Eq. (16), we get a profile of chemical potential within the diffusion layer. (See Appendix B)

$$\mu_{CP}(\eta) = \frac{RT\ V_{MAX}(H-S)}{16D}[6(\eta^2 - f^2) - (\eta^4 - f^4)] + \mu_{\eta=0} \tag{19}$$

Calculated projections of chemical potential based on Eq. (19) are shown in Fig. 3.

Profile of Chemical Potential and Concentration within Gel Layer (Zone C)

The gel layer ranges from $\mathrm{z} = 0$ to $\mathrm{z} = \mathrm{S}$. Within this layer transverse velocity is assumed to be constant being equal to $V_{GEL} = V_{MEMBR} = V_{MAX}$,

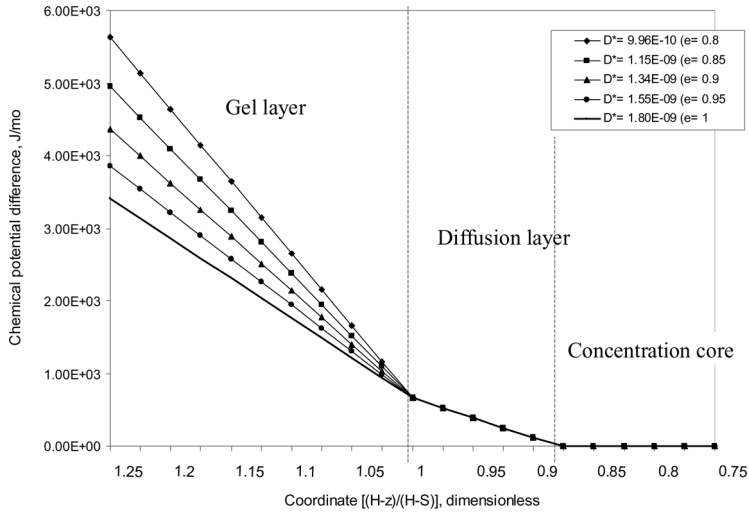

Figure 3. Calculated projections of chemical potential at different values of effective diffusivity within the gel layer (calculation for $D^*$is based on Eq. (7). Input data: $D = 1.8 \cdot 10^{-9}\,\mathrm{m^2/s}$; $V_{MEMBR} = 5 \cdot 10^{-6}\mathrm{m/s}$; $\mathrm{H} = 0.001\,\mathrm{m}$; $\mathrm{S} = 2 \cdot 10^{-4}\,\mathrm{m}$).

(see Fig. 1), thus Eq. (2) can be written for the gel layer as follows:

$$V_{GEL}c(z) + D^*_{GEL}\frac{dc}{dz} = 0 \tag{20}$$

Boundary conditions at the membrane surface (see Fig. 1) are:

$$C_{(Z=0)} = C_{1M}$$

And at the upper surface of gel layer are:

$$C_{(Z=S)} = C_{1G}$$

Rearrangement of Eq. (20) gives the concentration profile within the gel layer, $c(\theta)$, (see Appendix C). In terms of gel surface concentration-C_{1G}, it gives:

$$\frac{c(\theta)}{C_{1G}} = \exp\left[\frac{V_{GEL}}{D^*_{GEL}}S(1-\theta)\right] \tag{21}$$

Combining Eqs. (21) and (17) we express $\mathrm{G_{1G}}$ in terms of $\mathrm{G_1}$ that gives distribution of concentration within the gel layer, $c(\theta)$, in terms of the bulk concentration $\mathrm{C_1}$.

$$\frac{c(\theta)}{C_1} = \exp\left[\frac{5V_{MAX}}{8D}(H-S)(1-f^2)(5+f^2)\right]\exp\left[\frac{V_{GEL}}{D^*_{GEL}}S(1-\theta)\right] \quad (22)$$

At $\theta = 0$, Eq. (22) gives the CP module at membrane surface:

$$\left(\frac{C_{1M}}{C_1}\right)_{\theta=0} = \exp\left[\frac{5V_{MAX}}{8D}(H-S)(1-f^2)(5+f^2)\right]\exp\left[\frac{V_{GEL}}{D^*_{GEL}}S\right] \quad (23)$$

Differentiating Eq. (23) with respect to the θ-variable, we get an effective thermodynamic driving force within the gel layer, $-(d\mu/d\theta)_{P,T}$

$$\frac{d\mu_i}{d\theta} = RT\frac{d}{d\theta}[\ln c_i(\theta)] \quad (24)$$

Inserting the first derivative of the concentration profile, $c_i(\theta)$, Eq. (22), into Eq. (24) we get a profile of chemical potential within diffusion layer, $\mu_G(\theta)$. (See Appendix D)

$$\mu_G(\theta) = \frac{RTV_{MAX}S}{D^*}(1-\theta) + \frac{RTV_{MAX}(H-S)}{16\ D}(5-6f^2+f^4) + \mu_{\eta=0} \quad (25)$$

Calculated projections of concentration and chemical potential for zones (A), (B) and (C) based on Eq. (16), (19), (22), (25) are shown in Figs. 2 and 3.

RESULTS AND DISCUSSIONS

Calculated profiles in liquid phase and within gel layer, based on Eqs. (16) and (22), are shown in Fig. 2.

In the presence of the gel layer the membrane surface concentration, C_{1M}, is enhanced due to hindered back diffusion of salt ions that, in turn, results in growth of osmotic pressure and chemical potential at the membrane surface. The elevated surface concentration, C_{1M}, will also result in increase of salt concentration in permeate and decrease of the net driving force. Analysis of calculated data indicates high sensitivity of CP degree to coefficient of hindered back diffusion within the gel layer.

Model allows analyzing the influence of thickness and characteristics of fouling layer on the CP degree, surface concentration and profile of chemical potential. The Proposed model can be incorporated into the algorithm for calculation of the longitudinal distribution of CP degree, resistance, and trans-membrane flux.

CONCLUSIONS

The proposed model can be applied for quantitative analysis of processes accompanied by concentration polarization along with gel formation. It is essential for multi-component systems where the diffusion layer in the liquid phase and the gel (or cake) deposited at the membrane surface are built by different components. These layers are characterized by different values of effective diffusivity. The slope of the potential and concentration profile within the gel layer is higher than within the liquid phase that confirms the fact that the diffusion resistance within the gel layer is getting dominant and cannot be ignored. Calculated profiles in liquid phase and within the gel layer, based on Eqs. (16) and (22), are shown in Fig. 2. A sub-model describing the behavior of chemical potential can be applied in analysis of separation processes of multi-component solutions where the driving force should be expressed through ionic strength or chemical potential. The fouling potential of NOM, the behavior of fouling factors, the structure and morphology of the deposited layer are dependent upon chemical potential on the membrane surface.

Relying upon calculated data the following can be recommended for minimizing the negative impact of gel enhanced polarization in design of RO systems:

1. membrane with moderate degree of rejection rather than with the high one could be preferred on the first stage of RO;
2. nanofiltration could be recommended as a stage of the pretreatment before RO, that provides partial demineralization of the feed and makes the process less vulnerable to gel enhanced CP.

ACKNOWLEDGEMENTS

The author is grateful to the National Energy and Water Research Center (ADWEA) for supporting this study.

SYMBOLS AND ABBREVIATIONS

a	Activity, mol/m^3;
C	Concentration, mol/m^3;
D^*	Hindered diffusion coefficient within deposited gel layer, m^2/s;
D	Solute diffusivity in bulk, m^2/s;
e	Apparent porosity of deposited layer, dimensionless;

f_C	Upper boundary of diffusion layer in terms of the first dimensionless variable, $\eta = f_C$, dimensionless;
H	Half channel height, m
P	Operating pressure, Pa
S	Thickness of deposited fouling (gel) layer, m;
V_0	Trans-membrane velocity, m/s
V_{MEMBR}	Transverse velocity through membrane, m/s
V_{GEL}	Transverse velocity through deposited gel (or cake) layer, m/s
V_{MAX}	Transverse velocity at the membrane surface, m/s
δ_C	Thickness of diffusion layer, m
δ_W	Thickness of viscous layer, m
η	The first dimensionless variable, $\eta = (H - z)/(H - S)$
θ	The second dimensionless variable, $\theta = z/S$
π	Osmotic pressure, $\pi(s) = iCRT$, Pa
μ	Chemical potential, J/mol

Indexes

G	Gel (or cake) layer
1G	Gel surface
1M	Membrane surface
1	Bulk

REFERENCES

1. Hoek, E.M.V.; Kim, A.S.; Elimelech, M. (2002) Influence of cross-flow membrane filter geometry and shear rate on colloidal fouling in reverse osmosis and nano-filtration separation. *Environmental Engineering Science*, *19* (6): 357–372.
2. Hoek, E.M.V.; Elimelech, M. (2003) Cake enhanced concentration polarization: A new fouling mechanism for salt rejecting membranes. *Environmental Science and Technology*, *17*: 5581–5588.
3. Lee, S.; Cho, J.; Elimelech, M. (2004) Influence of colloidal fouling and feed water recoveryon salt rejection of RO and NF membranes. *Desalination*, *160*: 1–12.
4. Lee, S.; Cho, J.; Elimelech, M. (2005) Combined influence of natural organic matter (NOM) an colloidal particles on nanofiltration membrane fouling. *Journal of Membrane Science*, *262*: 27–41.
5. Chong, T.H.; Wong, F.S.; Fane, A.G. (2007) Enhanced concentration polarization by unstirred fouling layers in reverse osmosis: Detection by sodium chloride tracer response technique. *Journal of Membrane Science*, *287*: 198–210.
6. Herzberg, M.; Elimelech, M. (2007) Biofouling of reverse osmosis membranes; role of biofilm- enhanced osmotic pressure. *Journal of Membrane Science*, *295*: 11–20.

7. Kilduff, J.E.; Mattaraj, S.; Belfort, G. (2004) Flux decline during nanofiltration of naturally-occurring dissolved organic matter: effect of osmotic pressure, membrane permeability and cake formation. *Journal of Membrane Science*, *239*: 39–53.
8. Huertas, E.; Herzberg, M.; Oron, G.; Elimelech, M. (2008) Influence of biofouling on boron removal by nanofiltration and reverse osmosis membranes. *Journal of Membrane Science*, *318*: 264–270.
9. Agashichev, S. (2006) Enhancement of concentration polarization due to gel accumulated at membrane surface. *Journal of Membrane Science*, *285*: 96–101.
10. Berman, A.S. (1953) Laminar flow in channels with porous walls. *Journal of Applied Physics*, *24* (9): 1232–1235.
11. Boudreau, B.P. (1996) The diffusive tortuosity of fine-grained unlithified sediments. *Geochimica et Cosmochimica Acta*, *60* (16): 3139–3142.
12. Maerki, M.; Wehrli, B.; Dinkel, Ch.; Muller, B. (2004) The influence of tortuosity on molecular diffusion in freshwater sediments of nigh porosity. *Geochimica et Cosmochimica Acta*, *68* (7): 1519–1528.
13. Schlichting, H. (1974) *Grenzschicht-Theorie,* 5th Ed.; Verlag G. Braun.
14. Atkins, P.W. (1998) *Physical Chemistry,* 6th Ed.; Oxford University Press.

APPENDIX A: PROFILE OF CONCENTRATION WITHIN DIFFUSION BOUNDARY LAYER *(INTEGRATING EQ.* (15) *OVER ZONE (B)*

The diffusion layer ranges from $z = S$ to $z = \delta_C$, where the transverse velocity ranges from $V = V_{(\eta=f)}$ to $V = V_{\max(\eta=1)}$

Eq. (2) can be written as follows:

$$V(z)C(z) + D\frac{dC}{dz} = 0 \qquad \text{(A\_1)}$$

Boundary conditions at the upper boundary of diffusion layer (see Fig. 1) are:

$$C_{(Z=\delta_C)} = C_1$$

And at the upper boundary of the deposited layer:

$$C_{(Z=S)} = C_{1G}$$

For simplification of mathematical treatment the non-dimensional variable-η was used

$$\eta = \frac{(H - z)}{(H - S)} \qquad \text{(A\_2)}$$

Inserting transverse profile, Eq. (5), into Eq. (A_1) and combining with (A_2)) we get

$$V_{MAX}\frac{\eta}{2}(3-\eta^2)C(\eta)-\frac{D}{(H-S)}\frac{dC}{d\eta}=0 \tag{A_3}$$

Separation of variables gives

$$\frac{V_{MAX}}{D}\frac{(H-S)}{2}\int(3\eta-\eta^3)d\eta=\int\frac{dc}{c} \tag{A_4}$$

Having been integrated Eq. (A_4) gives

$$\frac{V_{MAX}(H-S)}{8D}(6\eta^2-\eta^4)=\ln c+const_{1C} \tag{A_5}$$

Evaluation of the constant of integration, $const_{1C}$

For the $const_1$ to be determined, we use the boundary conditions at the upper boundary of diffusion layer where $\eta=f=(1-Sc^{-1/3})$

$$C_{(\eta=f)}=C_1$$

It gives the $const_{1C}$.

$$const_{1C}=\frac{V_{MAX}(H-S)}{8D}(6f^2-f^4)-\ln C_1 \tag{A_6}$$

Inserting the $const_{1C}$ into Eq. (A_5) we get the following function for concentration profile within diffusion layer. (Within the range from $\eta=f$ to $\eta=1$ and from $C=C_1$ to $C=C_{1G}$)

$$\frac{c(\eta)}{C_1}=\exp\left\{\frac{V_{MAX}(H-S)}{8D}[6(\eta^2-f^2)-(\eta^4-f^4)]\right\} \tag{A_7}$$

APPENDIX B: PROFILE OF CHEMICAL POTENTIAL WITHIN DIFFUSION BOUNDARY LAYER *(INTEGRATING EQ.* (18) *OVER ZONE (B)*

An effective thermodynamic driving force, Eq. (18), in terms of the η variable:

$$\frac{d\mu_i}{d\eta}=RT\frac{d}{d\eta}[\ln c_i(\eta)] \tag{B_1}$$

Inserting the first derivative of concentration profile (Eq. 16) into Eq. (B_1) we get

$$\frac{d\mu}{d\eta} = \frac{RT\ V_{MAX}(H-S)}{4D}(3\mu - \eta^3) \qquad \text{(B\_2)}$$

Integrating of Eq. (B_2) gives

$$\mu_{CP}(\eta) = \frac{RTV_{MAX}(H-S)}{16D}(6\eta^2 - \eta^4) + const_{1M} \qquad \text{(B\_3)}$$

Evaluation of the Constant of Integration, $const_{1M}$

For the $const_{1M}$ to be estimated, we use the boundary conditions at the upper boundary of diffusion layer where $\eta = f$, therefore.

$$const_{1M} = \mu_{\eta=f} - K_{CP}\frac{(6f^2 - f^4)}{16} \qquad \text{(B\_4)}$$

Inserting the $const_{1M}$ into Eq. (B_3), it gives the profile of chemical potential within diffusion layer.

$$\mu_{CP}(\eta) = \frac{RTV_{MAX}(H-S)}{16D}[6(\eta^2 - f^2) - (\eta^4 - f^4)] + \mu_{\eta=f} \qquad \text{(B\_5)}$$

The potential within the concentration core having been assumed to be position – independent $\mu_{\eta=0} = \mu_{\eta=f}$ (see Assumptions), (B_5) gives the profile of chemical potential within diffusion layer.

$$\mu_{CP}(\eta) = \frac{RTV_{MAX}(H-S)}{16D}[6(\eta^2 - f^2) - (\eta^4 - f^4)] + \mu_{\eta=0} \qquad \text{(B\_6)}$$

APPENDIX C: PROFILE OF CONCENTRATION WITHIN THE GEL LAYER *(INTEGRATING EQ.* (20) *OVER ZONE (C)*

The gel layer ranges from z = 0 to z = S where the transverse velocity is assumed to be constant being equal to $V_{GEL} = V_{MEMBR} = V_{MAX}$, (see Fig. 1). The gel layer is characterized by hindered diffusivity, $D_{GEL}{}^*$, that

explains elevated values of diffusion resistance. Analysis of this zone is based on Eq. (20):

$$V_{GEL}c(z) + D^*_{GEL}\frac{dc}{dz} = 0 \qquad \text{(C\_1)}$$

Boundary conditions at the membrane surface (see Fig. 1) are:

$$C_{(Z=0)} = C_{1M}$$

And at the upper surface of gel layer are:

$$C_{(Z=S)} = C_{1G}$$

For simplification of mathematical treatment the non-dimensional variable, $\theta = z/S$, was used. After further rearrangement of Eq. (C_1) we get

$$\frac{V_{GEL}S}{D^*_{GEL}}d\theta = -\frac{dc}{c} \qquad \text{(C\_2)}$$

Integrating Eq. (C_2) gives

$$\ln\, c = -\frac{V_{GEL}S}{D^*_{GEL}}\theta + const_{2C} \qquad \text{(C\_3)}$$

Evaluation of the Constant of Integration, *const*$_{2C}$

The constant $const_{2C}$ is determined at the conditions that $C = C_{1G}$ at the upper surface of gel layer where $\theta = 1$ (z = S)

$$\text{Thus } const_{2C} = \ln\, C_{1G} + \frac{V_{GEL}}{D^*_{GEL}}S \qquad \text{(C\_4)}$$

Inserting the constant $const_{2C}$ into Eq. (C_3) we get

$$\ln_c(\theta) = \ln C_{1G} + \frac{V_{GEL}S}{D^*_{GEL}}(1-\theta) \qquad \text{(C\_5)}$$

Eq. (C_5) gives concentration profile within the gel layer

$$\frac{c(\theta)}{C_{1G}} = \exp\left[\frac{V_{GEL}S}{D^*_{GEL}}(1-\theta)\right] \qquad \text{(C\_6)}$$

Using Eq. (17) to express C_{1G} in terms of C_1 we get alternative formulation

$$\frac{c(\theta)}{C_1} = \exp\left[\frac{5V_{MAX}}{8D}(H-S)(1-f^2)(5+f^2)\right]\exp\left[\frac{V_{GEL}}{D^*_{GEL}}S(1-\theta)\right] \tag{C_7}$$

APPENDIX D: PROFILE OF CHEMICAL POTENTIAL WITHIN GEL LAYER *(INTEGRATING EQ.* (24) *OVER ZONE (C)*

An effective thermodynamic driving force expressed in terms of the θ variable as:

$$\frac{d\mu_i}{d\theta} = RT\frac{d}{d\theta}[\ln c_i(\theta)] \tag{D_1}$$

Inserting the first derivative of concentration profile (Eq. 22) into the right hand side of Eq. (D_1) we get

$$\frac{d\mu(\theta)}{d\theta} = -\frac{RTV_{MAX}S}{D^*} \tag{D_2}$$

Further integrating Eq. (D_2) gives.

$$\mu(\theta) = -\frac{RTV_{MAX}S}{D^*}\theta + const_{2M} \tag{D_3}$$

Evaluation of the Constant Integration, $const_{2M}$

The $const_2$ is determined for conditions at the upper boundary of gel layer implying the chemical equilibrium between component in the liquid phase and within the gel takes place, thus $\mu_{\theta=1} = \mu_{\eta=1}$

At $\theta = 1$ the Eq. (D_3) gives

$$\mu_{\theta=1} = -\frac{RTV_{MAX}S}{D^*} + const_{2M} \tag{D_4}$$

The chemical potential for component in liquid phase can be expressed from Eq. (19). At $\eta = 1$ it gives

$$\mu_{\eta=1} = \frac{RTV_{MAX}(H-S)}{16D}(5-6f^2+f^4) + \mu_{\eta=0} \tag{D_5}$$

Combining Eqs. (D_4) and (D_5) we get $const_{2M}$

$$const_{2M} = \frac{RTV_{MAX}(H-S)}{16D}(5 - 6f^2 + f^4) + \frac{RTV_{MAX}S}{D^*} + \mu_{\eta=0} \quad \text{(D\_6)}$$

Inserting the $const_{2M}$ (D_6) into Eq. (D_4) we get the distribution of chemical potential within gel layer

$$\mu_G(\theta) = \frac{RTV_{MAX}S}{D^*}(1-\theta) + \frac{RTV_{MAX}(H-S)}{16D}(5 - 6f^2 + f^4) + \mu_{\eta=0} \quad \text{(D\_7)}$$